Ion Kinetic Energy Distributions in a Compact ECR

Han-Ming Wu, David B. Graves*

Institute of Mechanics, Academia Sinica, Beijing 100080, China
**Dept. of Chemical Engineering, University of California, Berkeley, CA 94720*

Abstract: In the present paper, argon plasma behavior in a compact electron cyclotron resonance (ECR) reactor is studied by means of 2-D simulation. Using a hybrid electron fluid--particle ion model, we obtain ion kinetic energy and velocity distributions. In additional, neutral gas density effects are examined by the comparison between different pressures. Finally, the ion random kinetic energy of both parallel and perpendicular components, as well as velocity distributions are plotted

I Introduction

The application of electron cyclotron resonance (ECR) reactors in the microelectronics industry has appealed to some scientists and engineers for many years[1-3]. Much research work on ECR systems has been previously reported. In experimental work, some physical parameters were successfully measured by electrostatic probes[4-7]. In addition, the ion kinetic energy and ion velocity distributions were obtained by Doppler-shifted LIF (laser induced fluorescence) at several points in the plasma bulk[8-11]. In the previous modeling simulation works, several models were adopted, such as the particle model, the fluid model and the hybrid model [12,13,14].

In our previous work, a 2-D simulation code was developed and some interesting results were obtained(extended ECR)[15,16,17]. For example, changing some parameters of the source, such as power input and gas pressure, would change the plasma density, potential and electron temperature. These relations are obviously very useful to the ECR design.

The compact ECR plasma source seems to have more appeal because of its high etching rate and economic efficiency. In the present paper, we address operating characteristics variations affecting the ion kinetic energy distributions within the industrial operating parameter region. Some relations between gas pressure and ion kinetic energy distribution are studied by means of the comparison of the simulation results.

II Simulation Model

The geometry of the ECR plasma source and cylindrical coordinates (r,θ,z) are plotted in Fig 1. Wafer is supposed to put at the bottom Z=21.5 cm. The currents in the top magnetic coils and bottom coils are 160 A and 110 A, respectively. The top four coils are fixed and each coil has 164 turns. The bottom magnetic field is made up of four coils and each one has ten turns. The neutral pressure is assumed to be uniform with temperature 0.06 eV (1eV=11600ºK). The total microwave power input is 850 W with 2.45 GHz frequency.

(1) Particle ion model

The ions are treated as an individual particles. All the interaction between ions themselves are omitted. All new ions, with room temperature thermal velocity (0.06 eV), are created by electron-neutral ionization collisions which depend on the electron temperature and neutral gas density. When the ion hits the chamber wall it is taken out of the account. The ions move under the combined influence of the magnetic field and the plasma self-consistent static electrical field.

Ions have both elastic and charge-exchange collisions with the background neutral gas. The charge-exchange collision is assumed to be isotropic scattering whereas the elastic collision anisotropic. The absolute magnitudes of these two cross sections are considered almost the same. The charge-exchange collision cross section is assumed to be

$$\sigma_{ch} = 5.1 \times 10^{-19}\ m^2\ [1.6\text{-}0.048(\ln E)]^2$$

and elastic collision cross section

$$\sigma_{el} = 5.1\text{x } 10\ \text{-}19\ m^2\ [1.0\text{-}0.029(\ln E)]^2$$

where E is the ion total kinetic energy. For the elastic collision, the scattering angle is assumed to obey Gaussian distribution, i.e. the scattering angle probability distribution function is $\exp(-a\xi^2)$ where ξ is the scattering angle. Since such collision process is quite forward, it is reasonable to let a=100. This implies 95% of the collisions have the elastic scattering angle within five degrees. Because for the argon plasma, the ion mass and neutral mass is almost the same, the energy loss of the collision is $\varepsilon'=\varepsilon\cos^2\xi$ [18]. Each ion is described by 5-D phase space, i.e. $f(z,v_z,r,v_r,v_\theta)$, where z and r are axial and radial positions in cylindrical coordinates, v_z, v_r and v_θ are the three velocity components.

(2) Fluid electron model

Suppose the electron be a fluid and all electrons be in Maxwellian distribution. Most formulations we use here are taken from Golant, et al[19]. The detailed deduction can be found from ref[17]. For convenience, we give a brief introduction in the following.

For steady state, i.e. the derivative with respect to time is zero, the density balance, the momentum balance and the energy balance equations are written

$$\nabla\cdot\mathbf{J}_e = R_{ionz} \tag{1}$$

$$m_e n_e \nu_{en}\mathbf{u}_e = en_e(\nabla\phi - \mathbf{u}_e\times\mathbf{B}) - \nabla p_e - \gamma k\nabla T_e \tag{2}$$

$$\nabla\cdot\mathbf{Q}_e = e\mathbf{J}_e\cdot\mathbf{E} + P_{ecr} + P_{coll} \tag{3}$$

where J_e, R_{ionz}, T_e, n_e, n_n, m_e, ν_{en}, ϕ, γ, u_e, Q_e, P_{ecr} and P_{coll} are electron current density, ionization rate, electron temperature, electron density, neutral gas density, electron mass, electron-neutral collision frequency, plasma potential, adiabatic constant, electron velocity, electron energy flux, power input and the collision power loss, respectively. The power deposition profile is

$$P_{ecr}(z, r) = A[1.1-(r/R)^2]/[1-(B-B_0)^2/\delta B^2] \qquad (4)$$

where r is radial position, R device radius, B an applied magnetic field, δB=25 Gauss width of the resonant zone, B_0=950 Gauss resonant magnetic field and A a normalization constant. Eq(4) means that most power absorption is concentrated near the $B=B_0$ and r=0 region.

Electron-neutral collisional energy losses are included in the term P_{coll}:

$$P_{coll} = \Sigma R_i E_i = n_e n_n [k_{ionz}(T_e)E_{ionz}+k_{ex}(T_e)E_{ex}+k_m(T_e)E_m+k_{el}(T_e)E_{el}] \qquad [5]$$

where R_i is the rate $[m^{-3}s^{-1}]$ of *ith* process, E_i is the energy loss per collisional of *ith* type. On the right hand side of the equation, there are four types of collision energy losses we have considered here, i.e. ionization, excitation to resonant and metastable levels and elastic losses, respectively. The rate expressions are approximations based on integrating an assumed Maxwellian electron energy distribution function over a step function cross section.

The set of equations is closed with Poisson's equation relating the electron and ion densities to the electrostatic potential

$$\varepsilon_0 \Delta\phi = e(n_e - n_i) \qquad (7)$$

where ε_0 is the permitivity of vacuum and Δ the Laplace differential operator, respectively.

(3) Boundary conditions

In ECR systems, it is well known that the plasma sheath is so thin that either a non-uniform mesh is necessary or an extremely fine uniform mesh is required to resolve it numerically. However, the fine mesh in the sheath would significantly reduce the mean particle number in the spatial cell so that serious "noise" would appear in the ion density near the boundary. To avoid solving such a stiff problem, we suppose an analytical sheath of negligible thickness with the potential discontinuity $\delta\phi=\phi_s-\phi_w$, where ϕ_s is the potential at the plasma edge and ϕ_w the wall potential.

For the conducting wall, if the boundary is grounded, ϕ_w=0, otherwise it may be biased. The electron flux to the wall can be analytically expressed

$$\Phi_{ew}=0.25 n_e v_{eth} exp(-\delta\phi/T_e)\mathbf{b}\cdot\mathbf{n}$$

where v_{eth} is the electron thermal velocity, $\mathbf{b}=\mathbf{B}/B$ is a unit vector along the magnetic field direction and $\mathbf{n}$ a unit normal vector on the wall, respectively. The electron energy flux can be written in analogous way,

$$Q_{ew}=e v_{eth} T_e exp(-\delta\phi/T_e)\ \mathbf{b}\cdot\mathbf{n}/2$$

The density boundary condition is non-neutrality, i.e.

$$(n_i-n_e)/n_i = d$$

where d = 0.05.

For the dielectric wall, the surface potential will float with respect to ground. The ion and electron current balance requires

$$\Phi_{iw}=\Phi_{ew}=0.25 n_e v_{eth} exp(-\delta\phi/T_e)$$

so that the wall potential is

$$\phi_W=\phi_s+T_e ln(4\Phi_{iw}/n_e v_{eth})$$

III Results and discussions

(a) Constant neutral gas pressure

Figure 2 shows the spatial ion kinetic energy distribution with p_n = 5 mTorr. It is obvious that the ion kinetic energy near the walls is larger than that in the central area. This is because the potential gradient in the plasma pre-sheath gives energy to the ions and the gradient is higher near the walls. This kinetic energy consists of two components, i.e. directed and random components. Figures 3-4 show the ion directed kinetic energy and random kinetic energy with p_n=5 mTorr, respectively. The random kinetic energy can be decomposed into two components, perpendicular to magnetic line and parallel to magnetic line. Due to the relatively high potential gradient near the bottom, all these kinetic energy become larger and larger as they approach the bottom wall. Finally they are supposed to reach the Bohm velocities. Because our simulation grids are too coarse to describe the sheath structure, the real final kinetic value is supposed to be higher than the simulation results.

(b) Comparison between different gas pressures

Now let us see how the neutral gas pressure influences the ion kinetic behavior. Figure 5 is a plot of directed kinetic energy profiles on Z axis with p_n =1, 5 and 10 mTorr, respectively. Since both the radial component and the azimuthal component are negligible near the Z axis, the directed kinetic energy is approximately equal to the axial directed component. It can be seen that the axial directed kinetic energy is close to zero near the resonant zone. The resonant area is the peak of ion formation where their velocities are zero then they flow out in all directions. In comparison, axial directed kinetic energy increases more rapidly in lower pressure plasma. The electron temperature and plasma potential are higher at the lower neutral pressure, so the ions are more energetic.

Figure 6 is the ion random kinetic energy distributions on the Z axis with p_n = 1 and 5 mTorr, respectively. It is found that both parallel and perpendicular components in the higher gas pressure are relatively lower than the that in the lower pressure case. The positions of the minimum points for the parallel components are the same while the positions for the parallel components are different. Due to the higher T_e at the lower p_n, the plasma density gradient as well as the plasma potential gradient become larger as p_n goes down. Therefore, there are more energetic ions in the lower pressure case.

Figures 7-8 show the ion velocity distributions for neutral pressure 1 mTorr and 5 mTorr at the near wall point of Z=21 cm; respectively. It is well known that the velocity distribution width becomes wider and wider as the ions approach to the walls. It implies that the ion gains kinetic energy from the plasma static electric field during the period of its flight to the wafer at the bottom. The higher neutral pressure results in the more Maxwelllian-like velocity distribution.

References

[1] M.A.Lieberman & R.A.Gottscho, "Design of high density plasma source for materials processing," in *Phys. of Thin Films*, ed. M.Francombe & J.Voseen, Academic Press (1994).

[2] P.H.Singer, Semiconductor Inter., July,46(1991).

[3] J.Asmusser, *J.Vac. Sci. Tech.*, A7(3), 883(1989).

[4] S.M.Gorbakin, L.A.Berry and J.B.Roberto, *J. Vac. Sci. Tech.*, A8(3), 2983 (1990).

[5] J.L.Cecchi, J.E.Stevens, R.L.Jarecki,Jr. & Y.C.Huang, *J. Vac. Sci. Tech.*, B9(2), 318(1991).

[6] W. Holber and J. Forster , *J. Vac. Sci. Tech.*, A8(5), 3720(1990).

[7] R. A. Stewart, X.Y. Qian, D. A. Carl, B. Lake, Jr., J. Benasso, R. Lynch, C.A. Pico, M. A. Lieberman and N.W. Cheung, Memoradum No. UCB/ERL M90/100,12, November, 1990.

[8] E.A.Den Hartog, H. Persing & R. Claude Woods,*Appl.Phys.Lett.*,57(5), 661(1991).

[9] N.Sadeghi, T Nakano, D.J.Fravor & R.A.Gottscho, *J. Appl. Phys.*, 70, 2552(1991).

[10] T. Nakano, N.Sadeghi and R.A.Gottscho, *Appl. Phys. Lett.*, 58(5), 458(1991).

[11] R.Claude Woods, R.L.McClain, L.J.Mahoney, E.A.Den Hartog, H.Persing & J.S.Hamers, *Proc. Module Metrology, Control and Clustering*, 366(1991).

[12] M. A. Hussein and G. A. Emmert, *J. Vac. Sci. Tech.* , A8(3), 2913(1990).

[13] Y. Weng and M. J. Kushner, *J. Appl. Phys,.* (1992).

[14] M. A. Hussein, G. A. Emmert, N. Hershkowitz and R. Claude Woods, *J. Appl. Phys,.*72(5), 1720(1992).

[15] P.K.Porteous, H-M Wu & D.B.Graves, *Plasma Scources Sci. & Tech.*, 3 (1994)25.

[16] R.K.Porteous and D.B.Graves, *IEEE Tran. on Plasma Science,*19, 205(1991).

[17] H-M Wu, D. B. Graves and R.K. Porteous, *Plasma Sources Sci. & Technol,* (to be published)

[18] C. K. Birdsall and A. B. Langdon, *Plasma Physics & Computer Simulation* (McGraw Hill, New York, 1985).

[19] V. E. Golant, A. P. Zhilinsky, I. E. Sakharov and S. C. Brown, *Fundamentals of Plasma Physics*, John Wiley and Sons, New York, (1980).

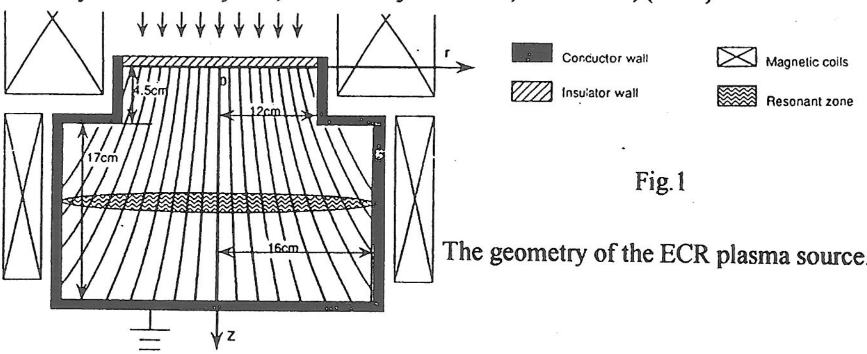

Fig.1

The geometry of the ECR plasma source.

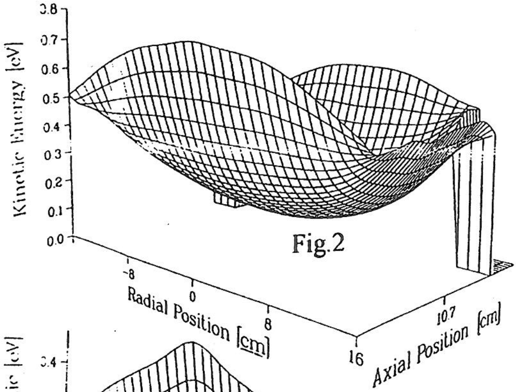

Fig.2

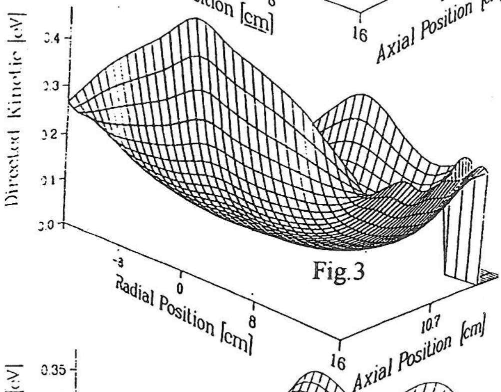

Fig.3

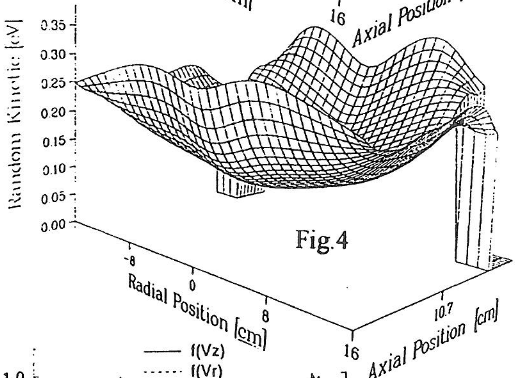

Fig.4

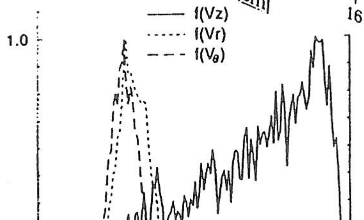

Fig.5

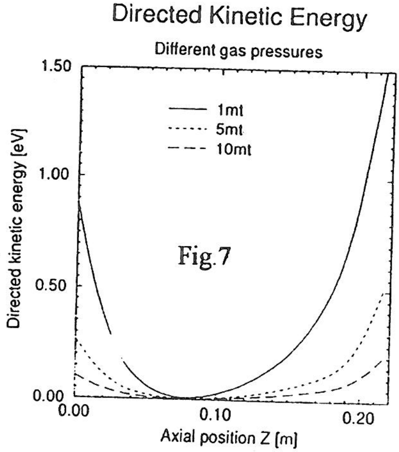

Fig.7

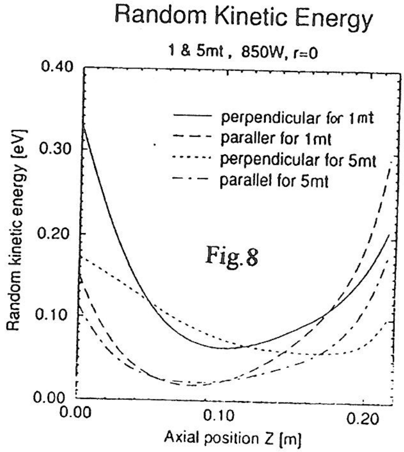

Fig.8

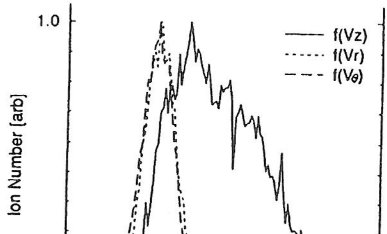

Fig.6